Sponge-Templated Preparation of High Surface Area Graphene with Ultrahigh Capacitive Deionization Performance

Zhi-Yu Yang, Lin-Jian Jin, Guo-Qian Lu, Qing-Qing Xiao, Yu-Xia Zhang, Lin Jing, Xiao-Xue Zhang, Yi-Ming Yan, and Ke-Ning Sun**

Capacitive deionization (CDI) is a competent water desalination technique offering an appropriate route to obtain clean water. However, a rational designed structure of the electrode materials is essentially required for achieving high CDI performance. Here, a novel sponge-templated strategy is developed for the first time to prepare graphene sheets with high specific surface area and suitable pore size distribution. Sponge is used as the support of graphene oxide to prevent the restack of graphene sheets, as well as to suppress the agglomerate during the annealing process. Importantly, the as-fabricated graphene sheets possess high specific surface area of 305 m^2 g^{-1} and wide pore size distribution. Ultrahigh CDI performance, a remarkable electrosorptive capacity of 4.95 mg g^{-1}, and siginificant desorption rate of 25 min, is achieved with the sponge-templated prepared graphene electrodes. This work provides an effective solution for the synthesis of rational graphene architectures for general applications in CDI, energy storage and conversion.

1. Introduction

Water treatment technologies, including water desalination and purification, have been considered as a key role to solve clean water shortage around the world. Reverse osmosis (RO) and thermal processes are commonly used to remove salts from water.[1] However, huge energy consuming and high costs have limited the large scale applications of these traditional deionization technologies. Recently, capacitive deionization (CDI), operating with low external power supply and energy consumption, has been emerged as a promising water desalination technique and provided an appropriate solution to obtain clean water.[2] As an electrochemical water treatment method, CDI is developed based on the principle of electric double-layer capacitor (EDLC). With a voltage supply, the electrodes can electro-adsorb the salt ions from the aqueous solution and stored them on the electrical double-layer region, that is, the internal porous electrodes surface. Thus, the CDI performance is largely depended on the physical properties and internal structure of the electrode materials, such as electrical conductivity, surface areas and pore size.

Generally, carbon materials, with high electrical conductivity and easily tunable structural property, have been considered as promising electrode materials for CDI. Various carbon materials, including graphene, carbon nanotube, activated carbon, carbon aerogel and their composites, have been investigated as CDI electrodes.[3] As an unique two dimensional structural material, graphene has been theoretically and experimentally demonstrated to possess superior CDI performance.[4] In particular, the theoretically high surface area, superior conductivity, mechanical properties and excellent chemical stability make graphene an ideal candidate for CDI application.[5] However, graphene sheets are prone to agglomerate during a typical reduction process of GO,[6] leading to uncontrollable pore size distribution and low surface area. Consequently, it decreases the EDLC of the electrodes and deteriorates the CDI performance. To circumvent this problem, different methods have been adopted to suppress the restacking of graphene sheets, thus enhancing their CDI performance. For example, graphene/mesoporous carbon composite was fabricated to form a mesoporous structure. Such composite showed an electrosorptive capacity of 0.73 mg g^{-1} at 2.0 V.[7] In another work, pyridine was used as the intercalating agent for exfoliation and reduction of graphene oxide, and the resultant graphene materials showed an electrosorptive capacity of 0.88 mg g^{-1}.[8] To enlarge the specific area, carbon nanotube (CNT) has been reported to combine with graphene. The obtained graphene-CNT exhibited electrosorptive capacity of 1.41 mg g^{-1}.[9] Recently, the resol was used to combine with graphene to alleviate the aggregation of graphene. The prepared electrode showed promising electrosorptive capacity of 3.47 mg g^{-1} at a voltage of 2.0 V.[10] Despite these achievements, essential efforts are needed to fully utilize the surface area and design the pore size of graphene to further improve the CDI performance. Towards these goals, graphene materials with

Dr. Z.-Y. Yang, L.-J. Jin, G.-Q. Lu, Q.-Q. Xiao, Dr. Y.-X. Zhang, Dr. L. Jing, X.-X. Zhang, Prof. Y.-M. Yan, Prof. K.-N. Sun
Beijing Key Laboratory for Chemical Power Source and Green Catalysis
School of Chemical Engineering and Environment
Beijing Institute of Technology
Beijing 100081, China
E-mail: yanym@bit.edu.cn; bitkeningsun@163.com

DOI: 10.1002/adfm.201304091

macroporous structure were developed. For instance, carbon nanotube-graphene hybrid aerogel were synthesized through supercritical CO_2 drying, possessing large surface area and high pore volume.[11] Moreover, three-dimensional macroporous graphene architecture with wide pore size distribution was fabricated by using polystyrene microspheres as sacrificial templates.[12] However, the synthetic strategies of these electrodes are relatively complicated, time-consuming, and practically high-cost. Therefore, it is highly desirable to develop a novel strategy to prepare graphene materials with characteristic structure, high surface area and rational pore size distribution for CDI applications.

Herein, we report for the first time on the sponge (polyurethane, PU)-templated strategy to prepare graphene with high surface area and favorable size distribution as CDI electrode materials. The obtained graphene composite has macroporous structure and exhibits a significantly high specific surface area of 305 m^2 g^{-1}, as well as a favorable pore size distribution larger than 3.5 nm. Moreover, we found that the prepared sponge-templated graphene (STGS) possesses high disorder and few layers of sheets. As expected, an ultrahigh electrosorptive capacity of 4.95 mg g^{-1} was obtained with STGS based CDI electrodes. As far as we know, this is the highest value among the ever-reported carbon based electrode materials for CDI applications.

2. Results and Discussion

2.1. Fabrication of Sponge-Templated Graphene Sheets

The strategy for the fabrication of STGS is illustrated in **Scheme 1**. Graphene oxide (GO) was firstly uniformly dispersed in water through a general ultrasonic treatment. Freshly washed sponge was then immersed into the above dispersion, and the color of sponge turned from yellow to black. After that, the sponge was took out, and dried. The procedure above was repeated several times. Finally, the sponge saturated with GO solution was annealed at 900 °C for 2 h at argon atmosphere, and a sponge-shaped graphene block was obtained.

2.2. Characterization of Sponge-Templated Graphene Sheets

To investigate the morphology of the as-prepared STGS, scanning electron microscopy (SEM) and transmission electron microscope (TEM) were presented in **Figure 1**. As shown in Figure 1a, STGS exhibits macroporous structure with well-defined interconnected pores at a size range from 76 μm to 379 μm. The high magnification SEM image in Figure 1b reveals clearly that the obtained 3D macroscope structure was comprised with layered graphene nanosheet. The composition of layered graphene nanosheets in STGS was verified by XRD patterns, as shown in Figure S1 (Supporting Information). Furthermore, the layered graphene nanosheets were confirmed by TEM image, as shown in Figure 1c. Figure 1d presents the HRTEM of STGS, revealing both ordered graphite lattices and disordered regions of STGS. The well-defined diffraction spots in selected area electron diffraction (SAED) confirm the crystalline structure of STGS, which is accordance with the previous report.[13] In a control experiment, the GN prepared without sponge template, as shown in Figure 1e,f, displays heavily agglomeration, indicating the restack of graphene sheets to graphite platelets. The different morphologies of two samples apparently imply the roles of sponge template. In order to further probe the function of sponge template, the sponge and sponge saturated with GO were also investigated with SEM, as shown in Figure S2a,b (Supporting Information). It can be seen that sponge shows many macropores interconnected with each other. After saturated with GO solution, the sponge skeleton was covered by GO and acted as a support of GO. Hence, it is believed that the skeleton of sponge was help to adsorb graphene sheets and prevent the agglomerate during the annealing process. Thereby, the sponge-templated strategy might offer an efficient way to prepare single or few layered graphene sheets with a rational 3D macroscopic architecture. It is known that the EDLC induced by the large exposed area can provide sufficient accessible area for ions absorption and accumulation and the space between the pores can serve as an efficient channel for fast mass transfer. Hence, we expect that the interconnected macroporous materials have high specific surface area, large porous space, as well as unique inner structure,

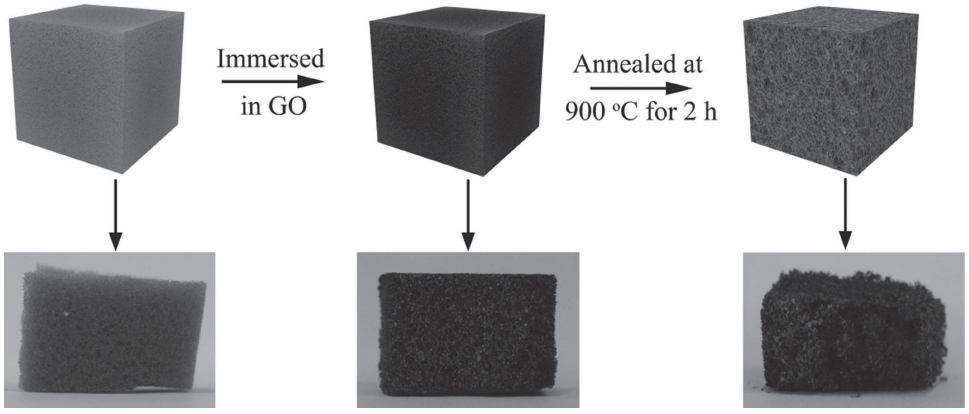

Scheme 1. Schematic representation of the procedure for preparing STGS sample. The down part gives the photo images of the sponge, sponge saturated with GO solution, and STGS.

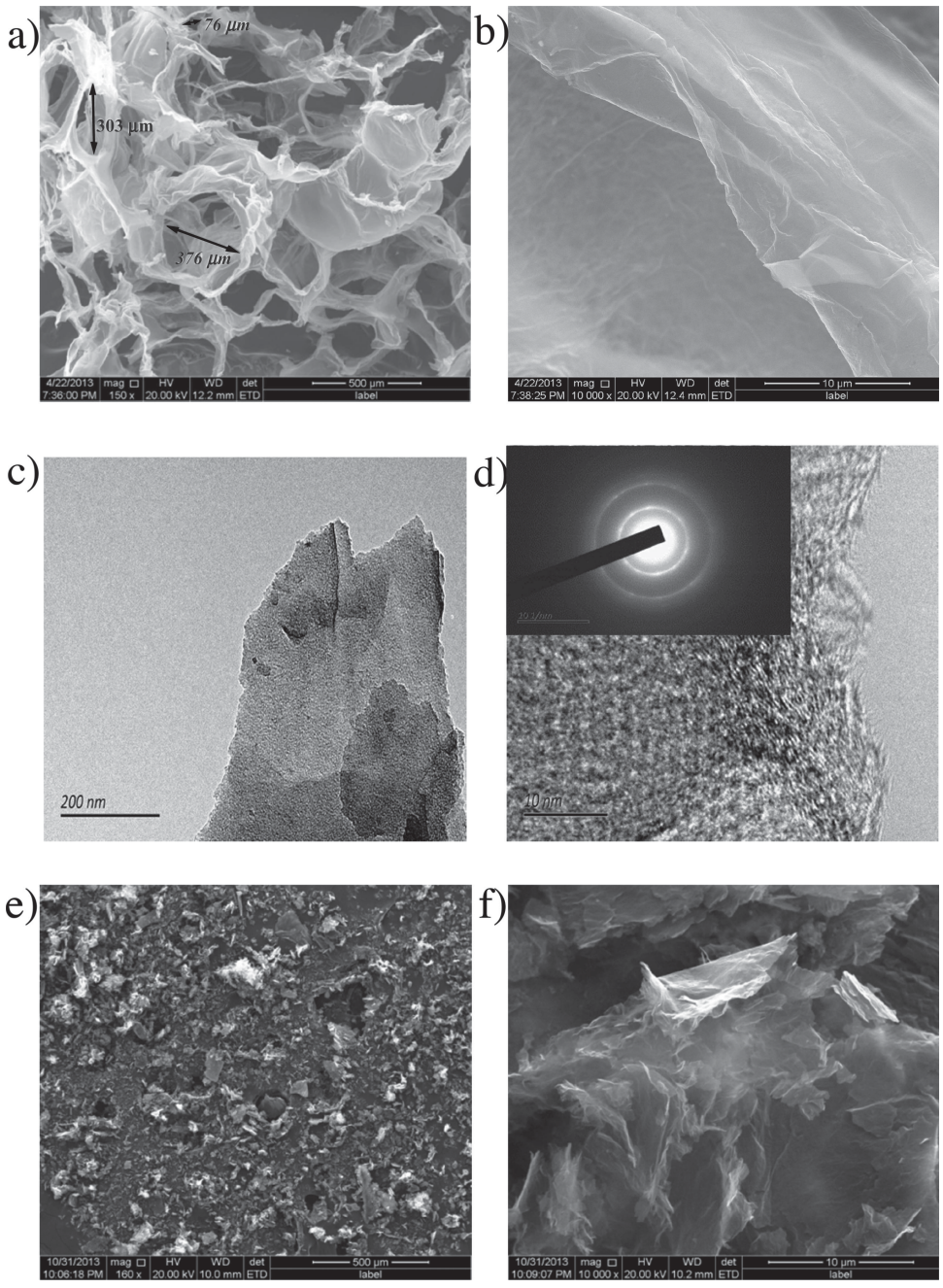

Figure 1. a,b) SEM images of STGS; c) TEM image of STGS; d) HRTEM image of STGS; The inset is the selected area electron diffraction pattern (SAED); e,f) SEM images of GN.

which are desirable for high performance supercapacitor and water desalination.

To further characterize the physical properties of STGS and verify the assumption above, more characterizations were performed. Large specific surface area and suitable pore size distribution is crucial for electrode materials. Therefore, N_2 adsorption/desorption analysis was performed and the results were presented in **Figure 2**a,b. Figure 2a shows that STGS has a specific surface area of 305 m^2 g^{-1}, which is higher than that of GN (178 m^2 g^{-1}) shown in Figure 2b. The high specific surface area of STGS is due to the reduced agglomeration of GN during the thermal treatment by using sponge template. Notably, under relative pressure of 0.45 P/P_0, no N_2 adsorbed on GN, whereas N_2 can still adsorb on STGS, indicating larger pore sizes existed in STGS. This could be revealed by the insets of Figure 2a,b, that the pores of STGS are larger than 3.5 nm and have a wide size distribution from 3.5 nm to 10 nm. As comparison, GN has the pores in sizes mainly less than 5 nm. To further characterize the pore structure of STGS, mercury penetration test was used to analyze the pore size distribution of STGS, from which a pore size distribution from 32.4 nm to 89.9 μm was confirmed, as shown in Figure 2c. For a control experiment,

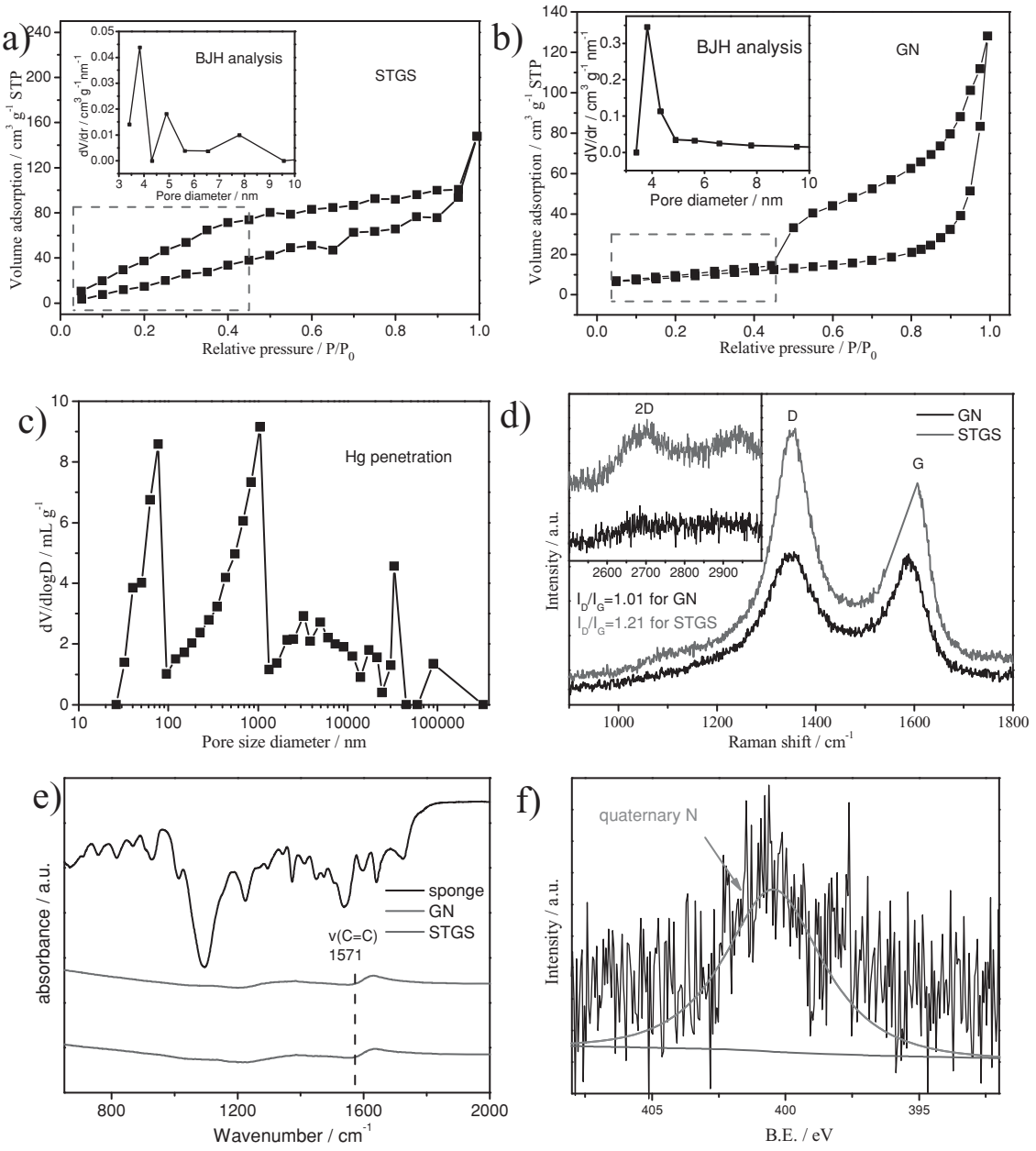

Figure 2. a,b) Nitrogen sorption isotherms and pore size distribution of STGS and GN samples; c) Mercury penetration curve of STGS sample; d) Raman spectra of STGS and GN; the inset shows an expanded view in the region of 2500–3000 cm^{-1}; e) FT-IR spectra for sponge, STGS and GN; f) High-resolution of N1s XPS spectra of STGS.

N_2 adsorption/desorption analysis was also performed on the product of annealed sponge, as shown in Figure S3 (Supporting Information). However, only a specific surface area of 27 m^2 g^{-1} was obtained, which is far lower than that of STGS. These results demonstrate that the sponge-assisted annealing strategy is an efficient way to obtain GN materials with enlarged specific surface area and a wide pore size distribution. To further confirm that sponge template helps to prevent the restack of graphene sheets, Raman spectroscopy was used to evaluate the thickness and graphitic quality of STGS and GN, shown in Figure 2d. The intensity ratio (I_D/I_G) of D band and G band for STGS is about 1.21, whereas the value of I_D/I_G for GN is only 1.01, implying that STGS possess much higher disordered graphitic structures compared with GN. Moreover, the 2D band could be used to identify the thickness of graphene sheets. A broader and asymmetric 2D band usually indicates an increased graphene layers. As shown in the inset of Figure 2d, a clearly sharp 2D band is observed for STGS in comparing to GN, suggesting a decrease of graphene sheets stacking, which is in accordance with the SEM images and BET results. Hence, the Raman results demonstrate STGS has a fewer layered and higher disordered graphitic structure than that of GN, implying sufficient exfoliation of graphene sheets by using sponge template. Such properties have been previously reported to help

improving the electrical conductivity.[12] Besides, Fourier transform infrared spectroscopy (FT-IR) was applied to examine the functional groups on sponge, STGS and GN samples. It can be seen, the peaks from 650 to 1800 cm^{-1} were clearly found for sponge sample. After pyrolysis with GO, the obtained STGS sample only showed a visible skeletal stretching vibration peak of aromatic C = C rings at 1571 cm^{-1}. In addition, we found that the FT-IR spectrum of STGS agrees well with GN. Thus, it is reasonable to believe that sponge completely pyrolysed during the preparation of STGS. X-ray photoelectron spectroscopy (XPS) spectrum was further conducted and presented in Figure 2f. The N1s spectrum of STGS reveals a peak centered at 400.5 eV, verifying the existence of quaternary N.[14] Combining the results obtained from FT-IR and XPS, a conclusion can be drawn that the pyrolysis of sponge during annealing process could nitridize graphene sheets. Previous work has reported that the electrical conductivity of GN can be improved through nitrogen doping.[15] Thus, the STGS is expected to have high electrical conductivity and promote the salty ions transfer. In addition, the sufficient exfoliation of graphene sheets may also contribute to rapid electrosorption and desorption of salty ions to the electrode.

To investigate the performance of STGS as supercapacitor electrodes, various electrochemical measurements were performed. Cycle voltammetry (CV) was first carried out to investigate the electrosorptive ability of STGS. **Figure 3**a,b displays CV curves of STGS and GN at different scan rates from 10 mV s^{-1} to 200 mV s^{-1} in 0.5 M NaCl aqueous solution. As seen, no redox reaction is observed in CV curves of STGS and GN, suggesting that they both act as typical EDLC based on the coulombic interactions rather than faradaic capacitance. Additionally, the CV curves of STGS exhibit rectangular shape, which means the charge current can reach the plateau quickly when applying reverse voltage. In other word, salty ions can fast and effectively adsorb to and desorb from the electrode. Even at 200 mV s^{-1}, rectangular shape of CV curves was nearly maintained, indicating rapid movement of ions into and out of STGS electrode at a high scan rate. In contrast, GN shows apparently inclined CV curves. The big difference between the CV curves of two graphene materials is probably attributed to their different interior structure. The macropores existed in STGS shorten the ion diffusion distance, leading to effective and fast ion diffusion. However, as demonstrated above, heavily restack of graphene sheets in GN suppressed the formation of pores, and the observed condensed structure of GN hinders the transfer of ions. The specific capacitance of electrode calculated from CV measurement can be used to evaluate the deionization efficiency. As shown in Figure 3c, the capacitance of STGS was calculated to be 57 F g^{-1} at 10 mV s^{-1} in 0.5 M NaCl solution, higher than that of GN (45 F g^{-1}). Even at 200 mV s^{-1}, STGS can exhibit a specific capacitance of 34 F g^{-1}, whereas GN only shows a value of 13 F g^{-1}. It means that STGS has better EDLC performance than GN towards salty ions accumulation. Meanwhile, the initial salt concentration has an effect on the electrical double layer thickness.[16] When the electrical double layer thickness is of similar magnitude as the pore size, the electrical double layer inside the pores overlaps, resulting in a loss of electrical capacity.[17] To examine this, CV measurements in NaCl aqueous solutions with different concentration (0.5–1.5 M) were performed. As shown in Figure 3d, the charged currents for both electrodes increased along with the increase of salt concentration. For comparison, the charge current calculated from CV curves of STGS electrode are much larger than those of GN at all different concentrations. It proves that STGS owns much better capacitive performance than GN. As shown in Figure 3e, along with the salt concentration from 0.5 M to 1.5 M, the calculated specific capacitances of STGS and GN change from 34 F g^{-1} to 47 F g^{-1}, and from 13 F g^{-1} to 24 F g^{-1} at a scan rate of 200 mV s^{-1}, respectively. We found that the specific capacitances of STGS increase relatively linearly with the concentration compared with that of GN. This phenomenon can be easily interpreted by the fact that STGS possesses larger pore size than GN, considering that larger pores can accommodate thicker electrical double layer, resulting larger specific capacitance.[15] In general, the well-defined electrochemical performance of the STGS based supercapacitor endows it with great advantages towards water desalination, owing to large specific surface area, wide pore size distribution and high electrical of STGS.

To further investigate the electrochemical properties of STGS and GN, equivalent series resistance (EIS) was performed. As shown in **Figure 4**a, the Nyquist plot of STGS displays relatively straight line, indicating a characteristic capacitive behavior at the low frequency region, which can be attributed to fast and easily diffusion of salty ions into the 3D macroporous. In contrast, GN shows an inclined line compared with STGS, implying poor diffusion behavior of the ions. The point intersecting the real axis in nyquist plots is referred to the value of the equivalent series resistance (ESR), including the electrolyte resistance, the internal electrode resistance and the electrical resistance between the electrode and the current collector. In general, small ESR value indicates low internal resistance and fast charge/discharge rate.[3d] As seen in Figure 4a, the ESR values obtained for STGS and for GN are 0.84 and 1.16 Ω, respectively. The small ESR for STGS is attributed to either the sufficient exfoliation or nitrogen doping effect realized with our sponge-templated strategy, which is beneficial for its application in CDI.

We next performed the galvanostatic charge/discharge (GC) of the two samples in a potential window from 0 V to 1 V at different current densities. Figure 4b shows the GC curves at the current density of 0.1 A g^{-1}. The GC curves of STGS and GN electrodes show classic triangular shapes with symmetric and linear lines, representing typical EDLC behavior and good reversibility. These features are crucial for high efficiency and long term operation of CDI. A close comparison shows that STGS has longer discharge time than GN does, implying that STGS possess higher specific capacitance than GN, which agrees well with the CV results above. In addition, the iR drop can be used to reveal the inner resistance of electrodes. Therefore, we examined the variation tendency of iR drop against the current density. As seen in Figure 4c, the iR drop increased linearly with the increase of current densities, which is in accordance with the previously reported work.[9] In particular, STGS shows smaller iR drop than GN in the whole range of different current densities, which is in agreement well with the EIS results above. Moreover, the durability is also a pivotal parameter for the long time working of CDI electrodes. Figure 4d presents the cycle stability test of two sample electrodes. Both

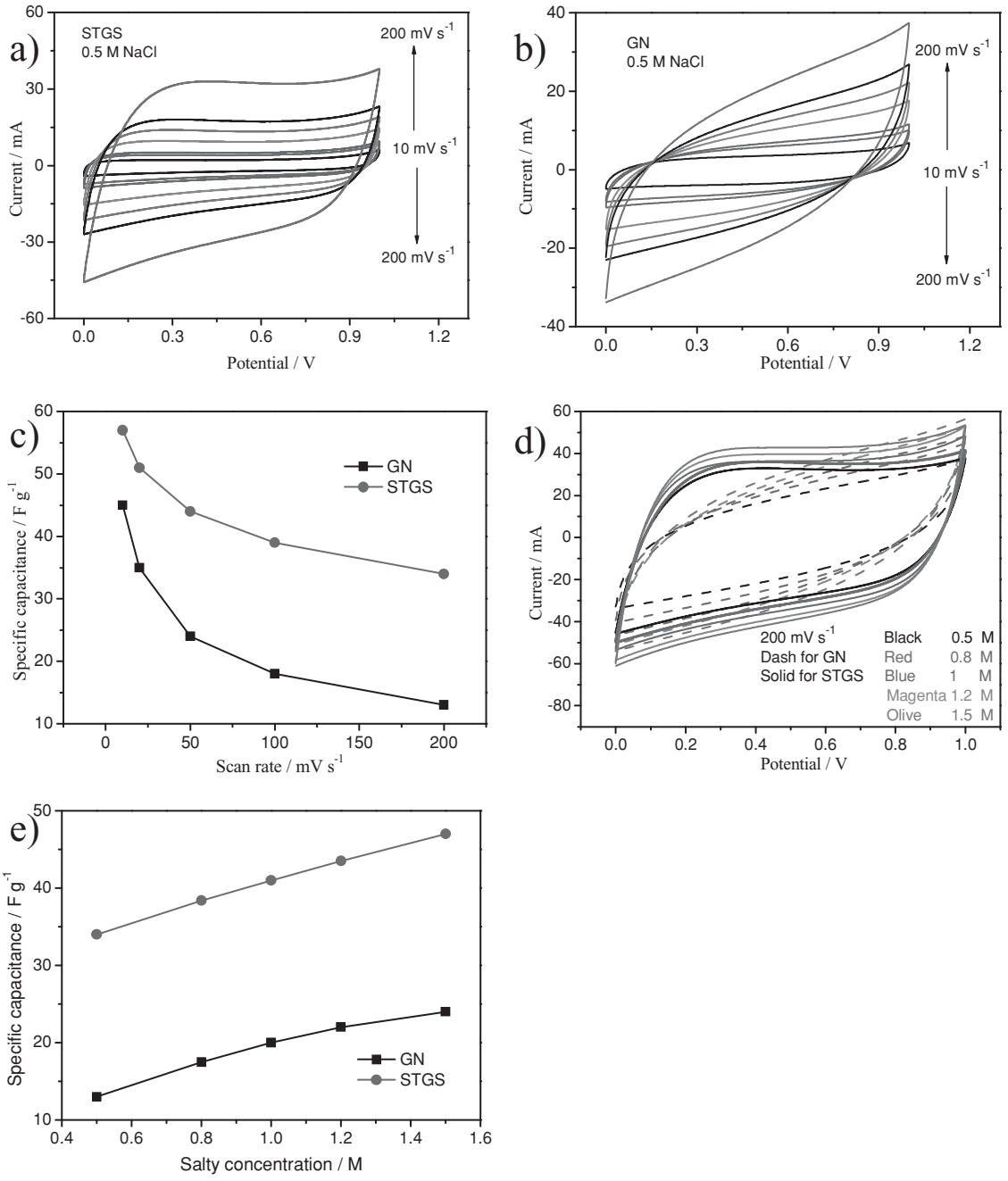

Figure 3. CV curves of a) STGS and b) GN at different scan rates in 0.5 M NaCl solution; c) Specific capacitance at different scan rates for STGS and GN in 0.5 M NaCl solution; d) CV curves of STGS and GN at 200 mV s^{-1} in different concentrations NaCl solution; e) Specific capacitance of STGS and GN in different concentrations NaCl solution.

STGS and GN electrodes exhibit promising stability. After 1000 cycles, the capacity retention for STGS and GN are 99.0% and 98.6%, respectively. We also examined the specific capacitance of STGS in 6 M KOH. According to the CVs, as shown in Figure S4, the specific capacitance of STGS was calculated to be 287 F g^{-1} at a scan rate of 10 mV s^{-1}, demonstrating the high capacitive properties of STGS. Combined with CV results, GC measurement, EIS analysis and stability testament, we conclude that obtained STGS with sponge-templated strategy show significantly improved electrochemical performance as supercapacitor electrodes. We attribute the enhanced performance to the utilization of sponge as template to assist the formation of macroporous structure. Such structure owns the advantages of large specific surface area and wide size distribution. As a consequence, it is anticipated that more salty ions could be electrosorped and accumulated in such a designed structure. Further, suitable sized pores may act as efficient channel for fast salty ions transfer, thus enhancing the reversibility. Importantly, the good durability of STGS may lead to promising long-term performance of CDI.

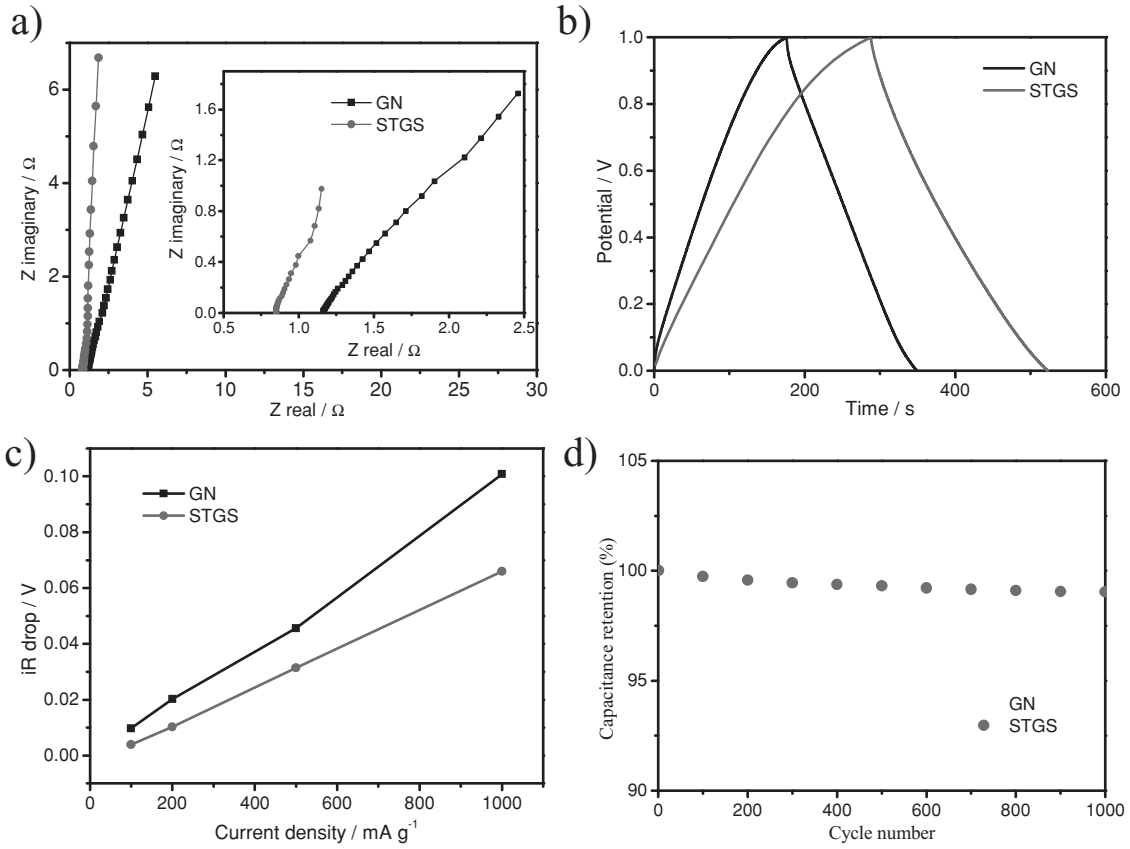

Figure 4. a) Complex plane plot of the impedance; inset: an expanded view in the region of high frequencies; b) GC curves of STGS and GN electrodes with a current density of 0.1 A g^{-1}; c) iR drop of STGS and GN at different discharge current densities; d) Variations of specific capacitance versus the cycle number with the current densities of 0.1 A g^{-1}.

To identify such assumptions, the capacitive deionization behavior of STGS and GN electrodes were carried out in 20 mL NaCl aqueous solution with an initial conductivity of 106 μS cm^{-1} and flow rate of 3 mL min^{-1}, as shown in **Figure 5**a. The applied voltage is 1.5 V and the desalination processes were carried out for 60 min. Figure 5b displays the variation of conductivity along with the desalination time. The conductivity of salty solution decreased quickly at the beginning of CDI processes, demonstrating a fast electrosorption of salty ions on electrode. With the time gonging on, the conductivity of solution decreases slowly, and reached to a stable value, suggesting an electrosorption equilibrium at the electrode. However, we noted that the descending rate of conductivity for STGS electrodes is faster than that of GN, indicating that salty ions are prone to be easily adsorbed at STGS electrode. Significantly, the electrosorptive capacities are calculated to be 4.95 mg g^{-1} and 2.85 mg g^{-1} for STGS and GN, respectively. In other word, STGS electrode can store much more salty ions than GN electrode does. For a comparison, the electrosorptive capacity for the annealed sponge sample is only 0.7 mg g^{-1} (Figure S5, Supporting Information). Moreover, we summarized the CDI performance of carbon based electrode materials reported in the literature, as shown in Table S1. Apparently, the electrosorptive capacity of the as-prepared STGS is higher than the reported results. To visualize the CDI effect, the morphologies of STGS before and after electrosorption tests were investigated with SEM. As can be seen in Figure S6 (Supporting Information), the surface of STGS before CDI test is very smooth, while a mass of particles was observed after electrosorption process, indicating salty ions have been substantially adsorbed on STGS. After desorption by a simple short circuit, most of the salty ions can be removed from STGS, as seen in Figure S6 (Supporting Information). We noted that the rapid desorption ability is as important as electrosorptive capacity, representing the regeneration rate of the electrode. Figure 5c presents two CDI cycles for STGS and GN electrodes. The regeneration process of STGS is only require 25 min, while desorption at GN electrodes need 30 min, indicating a high desorption efficiency of STGS electrodes. This can be convincely interpreted by the favorable porous structure with wide pore size, as well as large surface area of the STGS electrodes prepared with novel sponge-templated strategy.

3. Conclusion

In summary, we have successfully prepared sponge-templated graphene sheets (STGS) for the first time to achieve high surface area, suitable pore size distribution and low internal resistance for promising application in CDI. The obtained STGS electrodes have surface area of 305 m^2 g^{-1}, wide size distribution from 3.5 nm to 89.9 μm and low ESR value of 0.84 Ω.

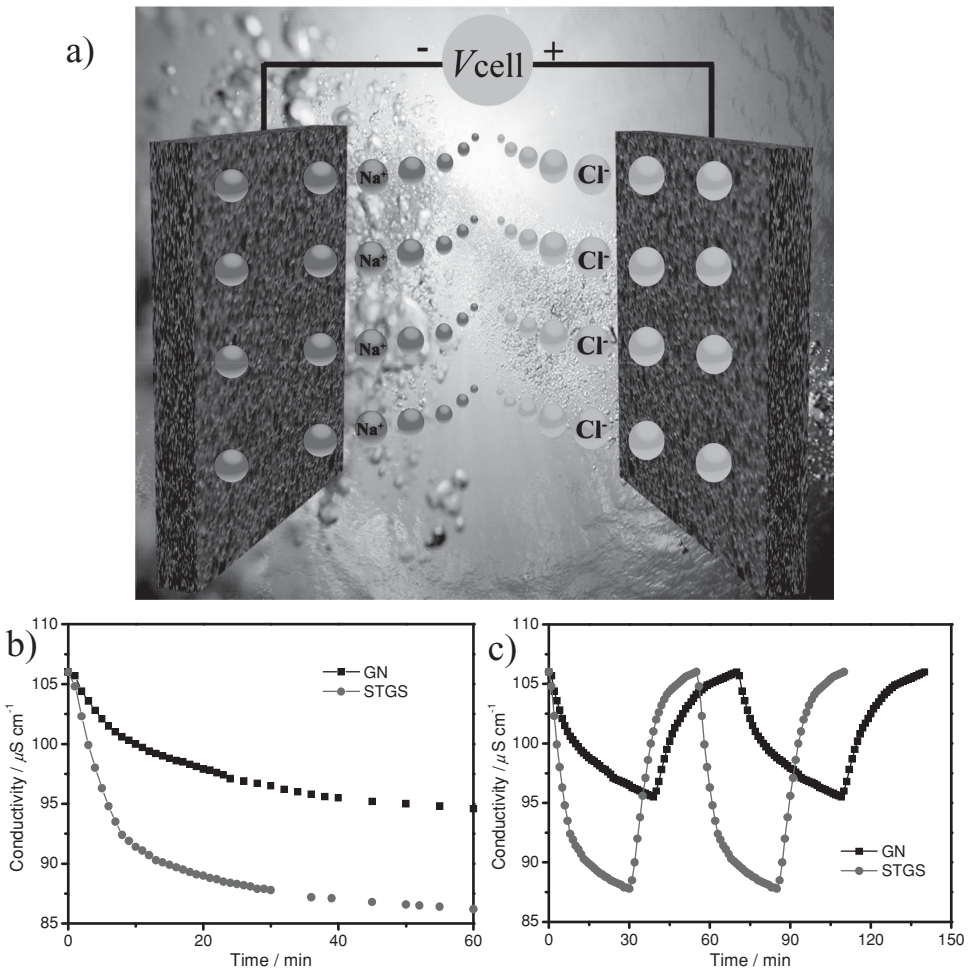

Figure 5. a) Schematic diagram of the CDI process; b) Variation of conductivity during the CDI process with an applied potential of 1.5 V; c) Adsorption/desorption profiles of STGS and GN electrodes.

The resulted macroporous materials composed of graphene nanosheets exhibited ultrahigh CDI performance with a superior electrosorptive capacity of 4.95 mg g^{-1} and a fast desorption rate of 25 min. The sponge-templated strategy offers a facile and variable route to rational design and prepare macroporous structured graphene-based electrode materials for a variety of applications in energy storage and conversion, catalysis and environmental treatment.

4. Experimental Section

Synthesis of the Sponge-Templated Graphene Sheets and Graphene: The graphite oxide (GO) was synthesized from natural graphite flake (Alfa Aesar, 325 mesh) by a modified Hummers method.[18] For synthesizing sponge-templated graphene sheets (STGS), 200 mg of GO was dispersed in 200 mL water. Freshly washed sponge was immersed into the above dispersion. After absorbing enough GO solution, the sponge was dried at 80 °C, repeatedly. Then the sponge saturated with GO was annealed at 900 °C for 2 h in an argon atmosphere. Graphene (GN) was prepared with directly annealing GO in the same procedure without sponge template.

Material Characterization: The morphology was characterized by scanning electron microscope (SEM, QUANTA FEG 250). Brunauer-Emmett-Teller (BET) measurements using N_2 absorption was performed on Autosorb-IQ2-MP-C system. Raman was performed on Renishaw RM 2000 with 633 nm laser. Fourier transform infrared spectroscopy (FT-IR) was performed (460 Plus, Jasco Japan) to investigate the functional group on sponge, STGS and GN. X-ray photoelectron spectroscopy (XPS, Physical Electronics 5400 ESCA) was used to quantitatively analyze the chemical compositions of GN-CNT.

Electrochemical Measurements: Electrochemical measurements were performed in three-electrode cell configuration on electrochemical analyzer (CHI660 instruments). Polytetrafluoroethylene (PTFE, Sigma-Aldrich; 60 wt% dispersion in water) was added to the mixture of samples and carbon black (samples / carbon / PTFE = 85 : 10 : 5 by weight) as a binder. The mixture was mixed into a paste using a mortar and pestle, and the slurry was pressed onto graphite paper and dried at 110 °C under vacuum for use as both the working and counter electrodes, respectively. The working and counter electrodes with nearly identical (by weight and size) were assembled in a test-cell with saturated calomel electrode as reference electrodes. The electrolyte was 0.5 M NaCl solution. For CDI process, a pairs of electrodes with an equal amount of STGS (or GN) separated by an insulating spacer was assembled to a water desalination model. The capacitive deionization behavior of STGS and GN electrodes were carried out in 20 mL NaCl

aqueous solution with an initial conductivity of 106 μS cm^{-1} and flow rate of 3 mL min^{-1}. The applied voltage is set as 1.5 V.

Supporting Information

Supporting Information is available from the Wiley Online Library or from the author.

Acknowledgements

Z.Y.Y. and L.J.J. contributed equally to this work. Financial support from the National Natural Science Foundation of China (Grant nos. 21175012), Ministry of Science and Technology (2012DFR40240) and the Chinese Ministry of Education (Project of New Century Excellent Talents in University) is gratefully acknowledged.

Received: December 6, 2013
Revised: January 14, 2014
Published online: March 4, 2014

[1] a) K. P. Lee, T. C. Arnot, D. Mattia, *J. Memb. Sci.* **2011**, *370*, 1; b) N. Misdan, W. J. Lau, A. F. Ismail, *Desalination* **2012**, *287*, 228; c) M. A. Shannon, P. W. Bohn, M. Elimelech, J. G. Georgiadis, B. J. Marinas, A. M. Mayes, *Nature* **2008**, *452*, 301.

[2] a) J. Benson, I. Kovalenko, S. Boukhalfa, D. Lashmore, M. Sanghadasa, G. Yushin, *Adv. Mater.* **2013**, *25*, 6625; b) H. Yin, S. Zhao, J. Wan, H. Tang, L. Chang, L. He, H. Zhao, Y. Gao, Z. Tang, *Adv. Mater.* **2013**, *25*, 6270; c) K. N. Knust, D. Hlushkou, R. K. Anand, U. Tallarek, R. M. Crooks, *Angew. Chem.* **2013**, *52*, 8107; d) M. Pasta, C. D. Wessells, Y. Cui, F. La Mantia, *Nano Lett.* **2012**, *12*, 839; e) M. D. Levi, N. Levy, S. Sigalov, G. Salitra, D. Aurbach, J. Maier, *J. Am. Chem. Soc.* **2010**, *132*, 13220; f) A. C. Pierre, G. M. Pajonk, *Chem. Rev.* **2002**, *102*, 4243; g) Y. Tao, H. Kanoh, L. Abrams, K. Kaneko, *Chem. Rev.* **2006**, *106*, 896; h) H. Strathmann, A. Grabowski, G. Eigenberger, *Ind. Eng. Chem. Res.* **2013**, *52*, 10364; i) T. Ryu, J. C. Ryu, J. Shin, D. H. Lee, Y. H. Kim, K.-S. Chung, *Ind. Eng. Chem. Res.* **2013**, *52*, 13738; j) P. Rana-Madaria, M. Nagarajan, C. Rajagopal, B. S. Garg, *Ind. Eng. Chem. Res.* **2005**, *44*, 6549.

[3] a) Y. Bouhadana, E. Avraham, M. Noked, M. Ben-Tzion, A. Soffer, D. Aurbach, *J. Phys. Chem. C* **2011**, *115*, 16567; b) I. Villar, S. Roldan, V. Ruiz, M. Granda, C. Blanco, R. Menéndez, R. Santamaría, *Energy Fuels* **2010**, *24*, 3329; c) P. M. Biesheuvel, B. van Limpt, A. van der Wal, *J. Phys. Chem. C* **2009**, *113*, 5636; d) C. J. Gabelich, T. D. Tran, I. H. M. Suffet, *Environ. Sci. Technol.* **2002**, *36*, 3010; e) C. Tsouris, R. Mayes, J. Kiggans, K. Sharma, S. Yiacoumi, D. DePaoli, S. Dai, *Environ. Sci. Technol.* **2011**, *45*, 10243; f) H. Li, L. Zou, L. Pan, Z. Sun, *Environ. Sci. Technol.* **2010**, *44*, 8692; g) S. Porada, L. Weinstein, R. Dash, A. van der Wal, M. Bryjak, Y. Gogotsi, P. M. Biesheuvel, *ACS Appl. Mater. Interfaces* **2012**, *4*, 1194.

[4] a) A. K. Geim, *Science* **2009**, *324*, 1530; b) A. R. Ranjbartoreh, B. Wang, X. Shen, G. Wang, *J. Appl. Phys.* **2011**, *109*; c) L. Zhuo, Y. Wu, W. Zhou, L. Wang, Y. Yu, X. Zhang, F. Zhao, *ACS Appl. Mater. Interfaces* **2013**, *5*, 7065; d) S. Zhang, Y. Shao, H. Liao, M. H. Engelhard, G. Yin, Y. Lin, *ACS Nano* **2011**, *5*, 1785; e) X. Huang, B. Sun, K. Li, S. Chen, G. Wang, *J. Mater. Chem. A* **2013**, *1*, 13484; f) S. Chen, P. Bao, G. Wang, *Nano Energy* **2013**, *2*, 425.

[5] D. Cohen-Tanugi, J. C. Grossman, *Nano Lett.* **2012**, *12*, 3602.

[6] a) F. Liu, M. Li, Q. Feng, N. Tang, W. Zhong, W. Huang, Y. Du, *Appl. Phys. Lett.* **2012**, 101; b) X. Yang, J. Zhu, L. Qiu, D. Li, *Adv. Mater.* **2011**, *23*, 2833.

[7] D. Zhang, X. Wen, L. Shi, T. Yan, J. Zhang, *Nanoscale* **2012**, *4*, 5440.

[8] H. Wang, D. Zhang, T. Yan, X. Wen, L. Shi, J. Zhang, *J. Mater. Chem.* **2012**, *22*, 23745.

[9] D. Zhang, T. Yan, L. Shi, Z. Peng, X. Wen, J. Zhang, *J. Mater. Chem.* **2012**, *22*, 14696.

[10] Z. Wang, L. Yue, Z.-T. Liu, Z.-H. Liu, Z. Hao, *J. Mater. Chem.* **2012**, *22*, 14101.

[11] Z. Sui, Q. Meng, X. Zhang, R. Ma, B. Cao, *J. Mater. Chem.* **2012**, *22*, 8767.

[12] H. Wang, D. Zhang, T. Yan, X. Wen, J. Zhang, L. Shi, Q. Zhong, *J. Mater. Chem. A* **2013**, *1*, 11778.

[13] G. Wang, J. Yang, J. Park, X. Gou, B. Wang, H. Liu, J. Yao, *J. Phys. Chem. C* **2008**, *112*, 8192.

[14] H. R. Byon, J. Suntivich, Y. Shao-Horn, *Chem. Mater.* **2011**, *23*, 3421.

[15] Y. Qiu, X. Zhang, S. Yang, *Phys. Chem. Chem. Phys.* **2011**, *13*, 12554.

[16] P. Xu, J. E. Drewes, D. Heil, G. Wang, *Water Res.* **2008**, *42*, 2605.

[17] K. L. Yang, T. Y. Ying, S. Yiacoumi, C. Tsouris, E. S. Vittoratos, *Langmuir* **2001**, *17*, 1961.

[18] W. S. Hummers, R. E. Offeman, *J. Am. Chem. Soc.* **1958**, *80*, 1339.